THE JOURNAL OF BIOLOGICAL CHEMISTRY
Vol. 280, No. 24, Issue of June 17, pp. 22925–22936, 2005
Printed in U.S.A.

Induction of the Nrf2-driven Antioxidant Response Confers Neuroprotection during Mitochondrial Stress *in Vivo**[S]

Received for publication, December 28, 2004, and in revised form, March 15, 2005
Published, JBC Papers in Press, April 19, 2005, DOI 10.1074/jbc.M414635200

Andy Y. Shih‡§¶, Sophie Imbeault‡§¶, Vilte Barakauskas‡§, Heidi Erb‡§, Lei Jiang‡§, Ping Li‡§, and Timothy H. Murphy‡§‖**

From the ‡Kinsmen Laboratory, Department of Psychiatry, §Brain Research Center, ¶Department of Physiology, University of British Columbia, Vancouver, British Columbia V6T 1Z3, Canada

NF-E2 related factor (Nrf2) controls a pleiotropic cellular defense, where multiple antioxidant/detoxification pathways are up-regulated in unison. Although small molecule inducers of Nrf2 activity have been reported to protect neurons *in vitro*, whether similar pathways can be accessed *in vivo* is not known. We have investigated whether *in vivo* toxicity of the mitochondrial complex II inhibitor 3-nitropropionic acid (3-NP) can be attenuated by constitutive and inducible Nrf2 activity. The absence of Nrf2 function in $Nrf2^{-/-}$ mice resulted in 3-NP hypersensitivity that became apparent with time and increasing dose, causing motor deficits and striatal lesions on a more rapid time scale than identically treated $Nrf2^{+/+}$ and $Nrf2^{+/-}$ controls. Striatal succinate dehydrogenase activity, the target of 3-NP, was inhibited to the same extent in all genotypes by a single acute dose of 3-NP, suggesting that brain concentrations of 3-NP were similar. Dietary supplementation with the Nrf2 inducer *tert*-butylhydroquinone attenuated 3-NP toxicity in $Nrf2^{+/-}$ mice, but not $Nrf2^{-/-}$, confirming the Nrf2-specific action of the inducer *in vivo*. Increased Nrf2 activity alone was sufficient to protect animals from 3-NP toxicity because intrastriatal adenovirus-mediated Nrf2 overexpression significantly reduced lesion size compared with green fluorescent protein overexpressing controls. In cultured astrocytes, 3-NP was found to increase Nrf2 activity leading to antioxidant response element-dependent gene expression providing a potential mechanism for the increased sensitivity of $Nrf2^{-/-}$ animals to 3-NP toxicity *in vivo*. We conclude that Nrf2 may underlie a feedback system limiting oxidative load during chronic metabolic stress

The Cap "n" Collar transcription factor NF-E2 related factor (Nrf2)[1] controls the coordinated expression of important antioxidant and detoxification genes (Phase 2 genes) through a promotor sequence termed the antioxidant response element (ARE) (1–3). Phase 2 genes work in synergy to constitute a pleiotropic cellular defense that scavenges reactive oxygen/nitrogen species (ROS/RNS), detoxifies electrophiles and xenobiotics, and maintains intracellular reducing potential (4–8). Normally, Nrf2 is sequestered in the cytoplasm by the actin-bound regulatory protein, Keap1 (9, 10). Multiple cysteine residues allow Keap1 to act as a molecular "switch" by responding to electrophiles/ROS with a conformational change, which releases Nrf2 for nuclear translocation and activation of Phase 2 gene expression (11–13). Thus, Nrf2 provides an important mechanistic link between oxidative stress leading to cell death and antioxidant gene expression supporting cell survival.

$Nrf2^{-/-}$ mice are particularly maladapted when challenged with toxicity paradigms such as hyperoxic lung injury, butylated hydroxytoluene-induced acute pulmonary injury, acetaminophen-induced liver toxicity, benzo[*a*]pyrene-induced tumorigenesis in the forestomach, or cigarette smoke-induced emphysema (14–19). Although the protective function of Nrf2 is apparent in peripheral tissues, the role of Nrf2 in the brain, where substantial ROS/RNS production can occur because of a high rate of metabolism, remains unclear. We hypothesize that Nrf2 function is critical for supporting neuronal survival during neurodegenerative disease when aberrant ROS/RNS production is known to be exacerbated (20). To study the effect of Nrf2 activity on *in vivo* neurodegeneration, we systemically administered 3-nitropropionic acid (3-NP), an irreversible inhibitor of succinate dehydrogenase (SDH), which causes striatal-specific cell loss leading to impairment of motor function (21). Metabolic inhibition by 3-NP produces oxidative stress in the brain through multiple mechanisms. 1) ATP depletion, membrane depolarization, increased neuronal/glial glutamate release, overactivation of *N*-methyl-D-aspartate ionotropic glutamate receptors, accumulation of intracellular Ca^{2+}, and excessive mitochondrial ROS production (22, 23). 2) Secondary activation of Ca^{2+}-dependent enzymes such as phospholipase A_2 (production of inflammatory mediators) and nitric-oxide synthase (peroxynitrite formation) (24, 25). 3) Excessive dopamine release, which can generate H_2O_2 when metabolized (26).

Up-regulation of Nrf2 activity in the brain is an attractive strategy for mitigating ROS/RNS overproduction during neurodegenerative disease. To test the hypothesis that augmenta-

* This work was supported by grants from the Canadian Stroke Network (to T. H. M.), Canadian Institutes of Health Research (to A. Y. S. and T. H. M.), Heart and Stroke Foundation of British Columbia (to T. H. M.), Michael Smith Foundation for Health Research (to A. Y. S., S. I., and T. H. M.), NSERC (to S. I.), and the Rick Hansen Institute (to A. Y. S.). The costs of publication of this article were defrayed in part by the payment of page charges. This article must therefore be hereby marked "*advertisement*" in accordance with 18 U.S.C. Section 1734 solely to indicate this fact.

[S] The on-line version of this article (available at http://www.jbc.org) contains Figs. S1 and S2.

¶ Both authors contributed equally to this work.

** To whom correspondence should be addressed: Dept. of Psychiatry, University of British Columbia, 4N1–2255 Wesbrook Mall, Vancouver, British Columbia V6T 1Z3, Canada. Tel.: 604-822-0705; Fax: 604-822-7981; E-mail: thmurphy@interchange.ubc.ca.

[1] The abbreviations used are: Nrf2, NF-E2 related factor; 3-NP, 3-nitropropionic acid; ARE, antioxidant response element; ROS/RNS, reactive oxygen species and reactive nitrogen species; tBHQ, *tertiary*-butylhydroquinone; SDH, succinate dehydrogenase; hPAP, heat-stable human placental alkaline phosphatase; NQO1, NA(D)PH:quinone oxidoreductase; GST, glutathione *S*-transferase; GCLC, γ-glutamylcysteine synthetase; xCT, cystine/glutamate exchanger; PBS, phosphate-buffered saline; LDH, lactate dehydrogenase; BSS, basic salt solution; ANOVA, analysis of variance; GFP, green fluorescent protein; RT, reverse transcriptase; HO-1, heme oxygenase-1; DN, dominant negative.

tion of Nrf2 could protect neurons *in vivo*, we increased Nrf2 activity in the brain using dietary administration of the small molecule inducer, *tert*-butylhydroquinone (tBHQ) or adenoviral-mediated overexpression of Nrf2 (6). In previous studies, these treatments protected cultured neurons from toxicity paradigms that mimic aspects of *in vivo* neurodegeneration, such as glutamate-induced glutathione depletion, dopamine toxicity, direct exposure to H_2O_2, metabolic inhibition with mitochondrial toxins (rotenone), platelet activating factor-induced inflammatory responses, and increased intracellular Ca^{2+} (6, 27–30). Importantly, neuronal cultures derived from $Nrf2^{-/-}$ mice showed increased susceptibility to neurotoxicity paradigms and were not protected by Nrf2 inducers, but could be rescued by overexpression of Nrf2 (27, 28).

Our *in vitro* and *in vivo* data suggest that Nrf2 activation is a protective response to counter the toxic effects of metabolic inhibition and ROS/RNS production in the brain. Loss of Nrf2 function in $Nrf2^{-/-}$ mice exacerbated motor deficits and striatal lesions caused by 3-NP administration. Conversely, preactivation of the Nrf2 response (using dietary administration of a Nrf2 inducer or viral gene transfer) attenuated 3-NP toxicity. Nrf2 activation may be a viable strategy to prime the antioxidant capacity of the brain, thereby decreasing injury caused by progressive neurodegeneration.

MATERIALS AND METHODS

Chemicals—All chemicals were obtained from Sigma unless otherwise stated.

In Vivo 3-NP Dosage Regimen—All experiments were approved by the University of British Columbia Animal Care Committee and were conducted in strict accordance with guidelines set by the Canadian Council on Animal Care. Adult male Wistar rats (Charles River, Canada) (250–350 g) and $Nrf2^{-/-}$ mice (C57Bl/6/SV129 background), originating from the laboratory of Dr. Yuet Wai Kan (32), were maintained in a 12-h light-dark cycle with food and water *ad libitum*. 3-NP was prepared in 0.1 M phosphate-buffered saline (PBS) and adjusted to pH 7.4 with NaOH and maintained at 4 °C for up to 1 week. For Nrf2 mice, a similar number of males and females (aged 10–16 weeks) were used. The 3-NP treatment regimen consisted of 9 total intraperitoneal injections with one injection given every 12 h at successively increasing doses: 20 mg/kg × 4, 40 mg/kg × 4, and 60 mg/kg × 1 (33). No significant difference was observed between males and females with respect to behavior, weight loss, or lesion size in this study. For rats, daily intraperitoneal injections of 3-NP ($n = 10$) or PBS control ($n = 10$) were administered by one of two dosage regimens: 40, 40, and 20 mg/kg or 40, 20, 20, and 20 mg/kg, each regimen resulting in the animal receiving a total of 100 mg/kg of 3-NP over 3 or 4 days. Both dosage regimens were tested to overcome possible preconditioning effects because of adenovirus injection. However, the average lesion volumes produced by the two dosage regimens were not different after statistical analyses (two-tailed *t* test), and the groups were pooled. Because virus was injected unilaterally we conservatively only included in the study animals with measurable 3-NP lesions by histology. Animals were sacrificed 24 h after the last injection or upon displaying severe motor behavior deficits such as recumbence (complete loss of motor control).

Semi-qualitative Behavior Scoring of Mice—A detailed description for the assessment of 3-NP induced motor deficits was described previously (33). Briefly, the scoring system involved the evaluation of 5 major symptoms each with a 3-tiered scoring scale (0, 1, or 2), with 0 = normal behavior and 2 = severe deficit. Symptoms included: (*a*) hind limb clasping, (*b*) reduced general locomotor activity, (*c*) hind limb dystonia (increased muscle tone leading to abnormal jerky movements), (*d*) truncal dystonia, and (*e*) postural instability. Animals received a cumulative score of 10 for each trial. Behavior was assessed by an experimenter blinded to the animal genotype and treatment before each scheduled injection.

Histology and Fluorojade Staining—Mice were deeply anesthetized with euthanyl (Bimeda-MTC) and trans-cardially perfused with room temperature PBS followed by ice-cold 4% paraformaldehyde in PBS. The brains were post-fixed overnight in paraformaldehyde and then cryoprotected with 30% sucrose for 2 days before cryostat sectioning. Cresyl violet staining was performed with standard protocols on 40-μm sections mounted on SuperFrost Plus slides (Fisher). Lesion volume was calculated according to the principle of Cavalieri (volume = $s_1d_1 + s_2d_2 + s_3d_3 + s_4d_4$), where s = lesion surface area and d = distance between the 2 sections. Adjacent 20-μm slide-mounted sections were examined for Fluorojade (Histochem Inc.) staining as previously described (34). Cresyl violet sections were scanned at 600 d.p.i. on an Epson desktop scanner and lesion area was quantified by an experimenter blinded to the animal genotypes using ImageJ software (National Institutes of Health). Four anatomical levels of the striatum were examined (Bregma (in mm) +1.10, +0.40, −0.26, −0.92) according to the mouse brain atlas (35). Fluorojade-positive neurons were only assessed in the core of the striatal lesion. Fluorojade images were collected using Northern Eclipse software (version 6.0). The wide-field fluorescence microscopy (Zeiss Axiophot) setup was equipped with a Retiga Exi CCD camera (QImaging). For rats, perfusion cryosectioning and cresyl violet staining were performed as described for mice. Total lesion volumes were calculated using the following formula $V_t = V_1 + V_2 + \ldots + V_n$, where $V_n = \pi h(r_{n-1}^2 + r_{n-1}r_n + r_n^2)/3$, where h is the distance between 2 sections and *r* is the radius of the lesion area using sections from Bregma (in mm) 1.70, 1.20, 0.70, 0.20, −0.26, and −0.80 according to the rat brain atlas (36).

Succinate Dehydrogenase Assay—Male or female mice from each genotype were acutely injected with 60 mg/kg of 3-NP and were always paired with PBS-injected littermates of the same sex and genotype. After 2 h, the mice were euthanized with halothane and then decapitated. Brains were washed with ice-cold PBS and striata and cortices were dissected from a 2-mm brain matrix slice at approximately Bregma +1.0 mm. Crude mitochondrial samples were prepared by Dounce homogenization in 0.25 M sucrose, 1 mg/ml bovine serum albumin, 1 mM EDTA, pH 7.4. To collect the mitochondria, the homogenate was centrifuged at 4 °C, 600 × *g* for 5 min. The supernatant was then re-centrifuged at 7,200 × *g* at 4 °C for 10 min. The supernatant was aspirated, and the mitochondrial pellet resuspended in the same buffer. SDH activity was assayed immediately using a protocol based on studies by Pennington *et al.* (37). Briefly, the reaction consisted of 0.1 M potassium phosphate buffer (pH 7.4), 0.1 M succinate, 0.05 M sucrose, 2 mg/ml *p*-iodonitrotetrazolium chloride (prepared fresh), and 125 μg/ml crude mitochondria (final concentrations in a 400-μl reaction volume) and incubated for 20 min at 37 °C. The formazan mixture was vortexed before measurement on a microplate reader at 490 nm. Protein concentration was measured using the bicinchronic acid method (Pierce). Brain homogenates were serially diluted for the assay and data analyses were performed on values within the linear range of the SDH reaction. We also used 4 $Nrf2^{+/-}$ mice to examine the dose-response relationship between acute SDH inhibition and various injected 3-NP concentrations (20, 40, or 60 mg/kg). Both 20 and 40 mg/kg doses produced little or no change 2 h after injection, compared with PBS injection (data not shown), whereas 60 mg/kg produced an observable decrease in activity. The 60 mg/kg dose was used for further SDH bioassays.

Preparation of tBHQ-supplemented Diets—All rats and mice were normally fed Lab Diet 5001, which contains no tBHQ, but trace amounts of BHA for preserving animal fats (2 ppm). For tBHQ feeding, food pellets were powdered in a coffee grinder and dry mixed with tBHQ (1% w/w). Distilled water was added to the powder (equal v/w), and the mixture was reshaped into food pellets. The pellets were then baked at 60 °C for 3 h. Control food was processed in the same fashion without the addition of tBHQ. Initially, we determined 5% tBHQ in diet was not consumed by $Nrf2^{+/-}$ mice ($n = 3$), and 0.5% tBHQ, although consumed, only slightly preserved motor function during 3-NP treatment ($n = 3$). For these reasons, a concentration of 1% tBHQ was used in all further feeding experiments.

Enzyme Assays for Brain Tissue—Brain and liver tissue were dissected in ice-cold PBS and homogenized with 10 strokes of a Dounce homogenizer in tissue buffer containing 25 mM Tris (pH 7.4) and 250 mM sucrose. Crude homogenates were centrifuged at 15,000 × *g* for 10 min at 4 °C. Tissue homogenate supernatants were collected and promptly assayed for enzyme activity. NQO1 enzyme activity was determined by calculating the dicumarol-sensitive fraction of 2,6-dichlorophenol-indo-phenol reduction (38). Reactions consisting of 25 mM Tris-HCl buffer (pH 7.4) with 0.7 mg/ml bovine serum albumin, 5 μM FAD, 200 μM NADH, 30 μg/ml protein, with and without 20 μM dicumarol were preincubated for 10 min at 25 °C (final concentrations in 200 μl of reaction volume). 2,6-dichlorophenol-indo-phenol was then added to a final concentration of 36 μM (20 μl volume), and the reaction was monitored at 540 nm. The extinction coefficient for 2,6-dichlorophenol-indo-phenol was $2.1 \times 10^4\ M^{-1}\ cm^{-1}$. The GST assay consisted of 1 mM 1-chloro-2,4-dinitrobenzene, 1 mM glutathione, and 100 μg/ml protein at 37 °C in 100 mM potassium phosphate buffer (pH 6.5) (final concentration in 150 μl of reaction volume) (39). The GST reaction was mon-

itored at 340 nm and the spontaneous non-enzymatic slope was subtracted from the total observed slope. The extinction coefficient for 1-chloro-2,4-dinitrobenzene was 9600 M^{-1} cm^{-1}. The lactate dehydrogenase (LDH) assay consisted of 3.3 mM pyruvate, 0.34 mM NADH, and 100 μg/ml protein in PBS at 37 °C (final concentrations in 150 μl of reaction volume) (40). The LDH reaction was monitored at 340 nm and the spontaneous non-enzymatic slope was subtracted from the total observed slope. Purified LDH enzyme standards were used to ensure that values were obtained within the linear range of the assay. The extinction coefficient for NADH was 6219 M^{-1} cm^{-1}. Protein concentration was determined using the bicinchronic acid method according to the manufacturer's protocol (Pierce).

Stereotaxic Injections—Rats were anesthetized by intraperitoneal injection of Somnitol (MTC Pharmaceuticals, Cambridge, ON) and placed in a stereotaxic frame (David Kopf Instruments). A burr hole was drilled and injection was performed into the right striatum at coordinates: 1.00-mm anterior-posterior from Bregma, 2.60-mm medial-lateral, and at both −4.50- and −5.50-mm dorsal-ventral, using a 10-μl Hamilton gas-tight syringe with a 26-gauge needle (type 2 tip). The virus was delivered by manually pressing the syringe plunger 3 times at 4-min intervals. Ad-GFP or Ad-Nrf2 was delivered at a concentration of 5×10^6 total plaque forming units in 3 μl of PBS. Wounds were irrigated with 0.9% sterile saline solution and sutured. Animals were allowed to recover for 3 days before 3-NP treatment was initiated.

Immunohistochemistry—For rats, frozen 10-μm brain sections were thawed in PBS for 3 min at room temperature. Mouse monoclonal anti-O4 (Chemicon) or rabbit polyclonal anti-glial fibrillary acid protein antibodies were diluted 1:400 and 1:200, respectively, in Ab buffer (3% bovine serum albumin and 0.3% Triton X-100 in PBS) and incubated overnight at 4 °C in a humid chamber. Sections were rinsed three times for 5 min in PBS and incubated with goat anti-mouse IgM Alexa 546-conjugated or goat anti-rabbit Alexa 546-conjugated secondary antibodies (both Molecular Probes, 1:500) in a humid chamber for 1 h at room temperature. Sections were rinsed three times for 10 min in PBS prior to mounting with Fluoromount-G (Southern Biotechnology Associates Inc.) and No. 1 glass coverslips (Corning). All GFP fluorescence from viral infection could be detected without using an anti-GFP antibody. To assess total striatal volume, a propidium iodide counterstain was used to label all cell nuclei. Sections were incubated in 8 μM propidium iodide dissolved in PBS for 10 min at room temperature followed by a 10-min PBS rinse. To determine infectivity, GFP fluorescence was calculated by thresholding images to subtract background and calculating the area of fluorescence (Image J). In the same section, propidium iodide staining was used to locate the corpus callosum and caudate putamen. The area encompassed by these two regions was defined as the striatal area. Data were expressed as % GFP^+ volume within the total striatal volume. For NeuN staining, an antigen retrieval process was used following thawing. Sections were incubated at 80 °C for 30 min in 10 mM sodium citrate (pH 8.5) and then rinsed for 5 min in PBS prior to anti-NeuN antibody incubation overnight at 4 °C (Chemicon, 1:100) and goat anti-mouse Cy3 secondary antibodies for 1 h at room temperature (Sigma, 1:200). Fluorescent images were captured using a Zeiss LSM Meta 510 confocal microscope and analyzed using NIH Image (for Mac) or ImageJ (for PC).

Preparation of Primary Glial-enriched and COS-1 Cultures—Enriched glial cultures were prepared from 0–2 day post-natal Wistar rat pups as described previously (6). The conditions used largely results in a population of Type I and II astrocytes as assessed by anti-glial fibrillary acid protein staining. COS-1 cells (ATCC) were maintained in Dulbecco's modified Eagle's medium supplemented with 10% fetal bovine serum, 1 mM sodium pyruvate, 2 mM glutamine, 100 units/ml penicillin, and 0.1 mg/ml streptomycin.

Plasmids and Adenoviruses—PEF mammalian expression plasmids carrying cDNA encoding mouse Nrf2 and Nrf2DN were a generous gift from Dr. Jawed Alam (Alton Ochsner Medical Foundation, New Orleans, LA) (1). Rat ARE sequences were obtained from the *nqo1* promotor. The human placental alkaline phosphatase (hPAP) reporter plasmid (rQR51) was constructed as described previously (6, 41). Recombinant adenoviral vectors were generated using the Cre-lox system (Canadian Stroke Network core facility, University of Ottawa), as described previously (6, 42). The N terminus-tagged Nrf2-GFP vector was made by PCR amplifying the Nrf2 coding sequence from the PEF vector with specific primer sequences: forward, 5′-ACTCAGATCTCGAGAAGATTTGATTGACATCCTT-3′, and reverse, 5′-CCCGGGGGTACCCTAGTTTTTTCTTTGTATC-3′. The resulting PCR product was restriction digested with XhoI and KpnI for ligation into the pEGFP-N1 vector (Invitrogen). The Keap1 vector was a generous gift from Dr. Masayuki Yamamoto (University of Tsukuba), later modified to Keap1-FLAG by Laurie Zipper (University of Wisconsin) (9, 43).

Transfection, Infection, and Treatments for Astrocytes and COS-1 Cells—Astrocytes and COS-1 cells seeded (1×10^5 cells/ml) in 24-well plates were transfected using Lipofectamine 2000 (Invitrogen), according to the manufacturer's protocol with some modifications. In particular, for each well of a 24-well plate, 1 μg of DNA and 1 μl of Lipofectamine were used. The transfection efficiency was typically ~20% for astrocytes and ~50% for COS-1 cells as assessed by β-galactosidase staining. For some experiments, adenovirus infection of astrocytes as described previously (6), was initiated immediately after Lipofectamine transfection. All infected cultures were examined for adequate infection efficiency (~90% of glia) as assessed by GFP fluorescence. 3-NP or tBHQ treatments were initiated 24 h after transfection.

3-NP was prepared in basic salt solution (BSS) consisting of (in mM) 3.1 KCl, 134 NaCl, 2.5 $CaCl_2$, 1 $MgSO_4$, 0.25 KH_2PO_4, 15.7 $NaHCO_3$ (pH 7.2), and filtered before use. The 3-NP stock was further diluted in BSS to the indicated concentration for experiments. Cells were washed with BSS twice and then exposed to 3-NP or BSS (vehicle) for 2 h. The cells were washed again 3 times with BSS and the original culture media was replaced. The Nrf2 inducer, tBHQ, was dissolved as a ×1000 concentrated stock in pure Me_2SO (vehicle), sterile filtered, and then diluted to a final concentration of 10 or 20 μM in the glial culture media. TBHQ was present in the media for the duration of the experiment until cells were harvested.

Placental Alkaline Phosphatase Assay—hPAP activity was measured as described previously (44). Briefly, cultures were collected in lysis buffer consisting of 10 mM Tris-HCl (pH 8), 1 mM $MgCl_2$, and 0.1% Triton X-100. Half of the sample was saved for determination of protein concentration and β-galactosidase activity (for normalization of transfection efficiency). The remaining sample was heated to 65 °C for 30 min to inactivate endogenous phosphatase activity. The assay was initiated by mixing ~15 μg of protein with diethanolamine buffer (0.73 M diethanolamine with 0.36 mM $MgCl_2$, pH 9.8), and 13.6 mM *p*-nitrophenyl phosphate (final concentrations in 150 μl reaction volume). The reaction was monitored every 2 min over 30 min, at 405 nm. For all assays, hPAP activity from rQR51mut-transfected astrocytes was subtracted as ARE-independent background.

Semi-qualitative Reverse-transcriptase PCR—Total RNA was isolated from infected cultures using TRIzol Reagent (Invitrogen) following the manufacturer's instructions. One μg of RNA was reverse transcribed using random hexamer primers and Thermoscript reverse transcriptase enzyme (Invitrogen). The resulting cDNA was then amplified by PCR using various primer sets (27): mouse Nrf2 exon 5, 5′-TCTCCTCGCTGGAAAAAGAA-3′ and 5′-AATGTGCTGGCTGTGCTTTA-3′; *nqo1*, 5′-CATTCTGAAAGGCTGGTTTGA-3′ and 5′-CTAGCTTTGATCTGGTTGTCAG-3′; *Xct*, 5′- TTGCAAGCTCACAGCAATTC-3′ and 5′-CGTCAGAGGATGCAAAACAA-3′; *gclc*, 5′-ACAAGCACCCCCGCTTCGGT-3′ and 5′-CTCCAGGCCTCTCTCCTCCC-3′; *β-actin*, 5′-CCCAGAGCAAGAGAGGTATC-3′ and 5′-AGAGCATAGCCCTCGTAGAT-3′.

PCR conditions were as follows: initial denaturing step using 1 cycle at 95 °C for 3 min, followed by 26 cycles at 95 °C for 30 s, the appropriate primer annealing temperature (~55 °C) for 40 s, 72 °C for 1 min, and a final cycle at 72 °C for 5 min. For *Xct* and *gclc*, 36 and 31 cycles were used, respectively. The PCR products were separated on a 1.4% agarose gel containing ethidium bromide. cDNA was then visualized using an ultraviolet light source. cDNA templates for each sample were serially diluted and band densities were plotted. These plots were used to ensure that data represented PCR products within the linear range of the reaction (supplemental materials Fig. 2).

Glutathione Assay—Total glutathione was quantified in glial cell lysates and tissue homogenates (0.3 mg/ml) by the method of Tietze (45), as described previously (6).

Western Blot Analysis and Immunocytochemistry—Western blot and immunocytochemistry was performed as described previously (6). Antibodies used include: rabbit anti-heme oxygenase 1 (Stressgen Inc., 1:500), goat anti-actin (Santa Cruz, 1:1000), sheep anti-rabbit horseradish peroxidase (Amersham Biosciences, 1:5000), donkey anti-goat horseradish peroxidase (Santa Cruz, 1:5000), mouse anti-FLAG M5 (Sigma, 1:1000), and goat anti-rabbit Texas Red (Molecular Probes, 1:2000).

Nrf2-GFP Localization in COS-1 Cells—After 2 h of 3-NP treatment or 4 h of tBHQ treatment, COS-1 cells were fixed and stained. Cell counting (and nucleus/cytoplasm delineation) was performed by an experimenter blinded to the treatment groups and directed to assess whether Nrf2-GFP fluorescence was excluded from or enriched in the nucleus. We did confirmatory experiments using a nuclear counterstain (Hoechst) and found in all other experiments that it was relatively straightforward to assess Nrf2 localization even without the counterstain because COS-1

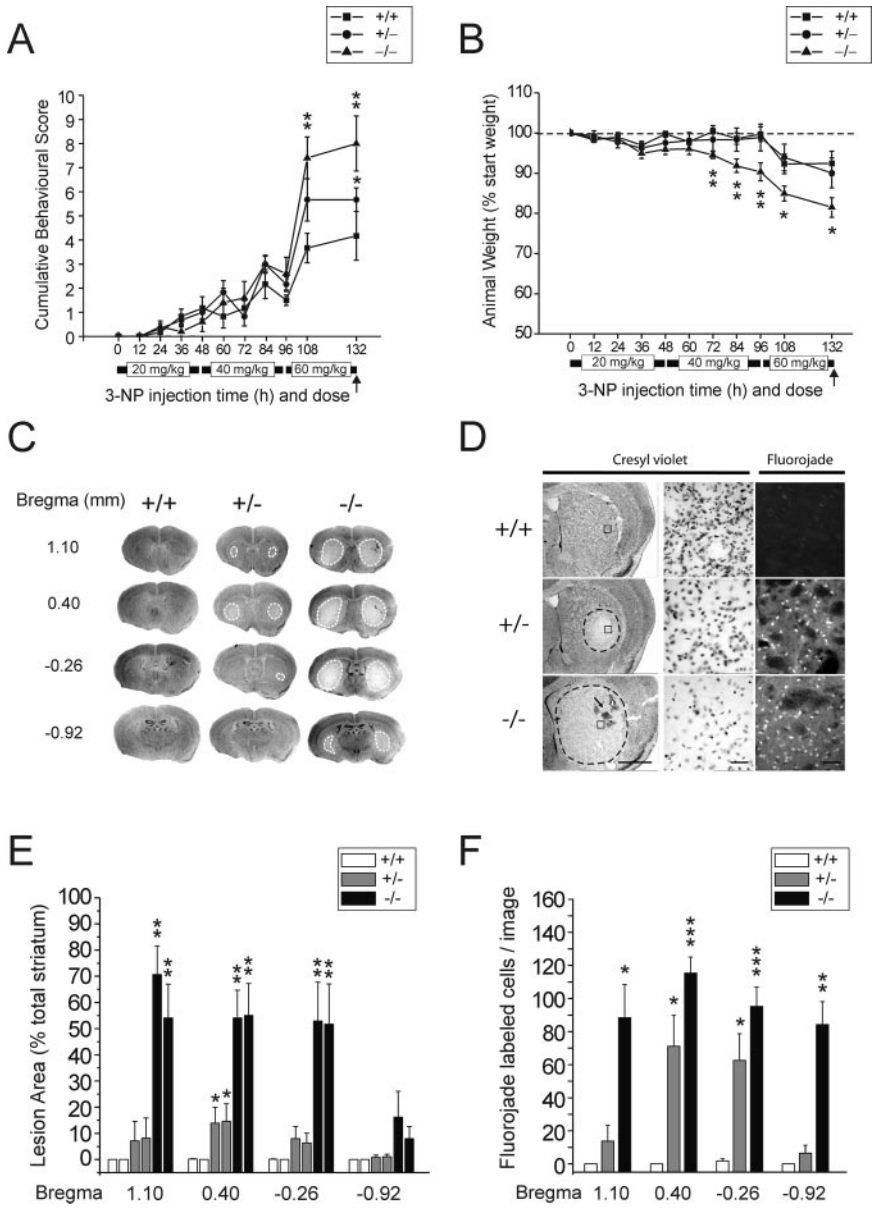

FIG. 1. **Behavioral scoring, weight loss, and lesions of mice with varied Nrf2 genotype during 3-NP challenge.** Behavior (*A*) and weight (*B*) were evaluated before each scheduled injection. The 3-NP treatment regimen consisted of 9 total intraperitoneal injections with one injection given every 12 h at successively increasing doses: 20 mg/kg × 4, 40 mg/kg × 4, and 60 mg/kg × 1 (doses are depicted with *black bars below* the *x* axis). At 108 h, behavior was measured but no injections were made. All animals were sacrificed 1.5 days after the last dose of 3-NP (*arrow*). *C*, representative cresyl violet-stained slices from all genotypes after 3-NP treatment. Pallor in staining because of cell death and cell shrinkage is outlined by *dotted lines*. *D*, representative images from cresyl violet-stained slices (*left column*, *scale bar* = 1 mm), magnified image from cresyl violet striatal inset (*middle column*, *scale bar* = 100 μm), and magnified image of Fluorojade staining (marker of neuronal degeneration) from striatal inset (*right column*, *scale bar* = 100 μm). *Arrow* shows typical hemorrhaging seen in some cases with the Nrf2$^{-/-}$ group. *E*, lesion area from 4 different levels relative to Bregma within the striatum were measured and expressed as percentage of total ipsilateral striatum. *Left* and *right bars* for each genotype correspond to left and right hemispheres. No significant differences were seen between hemispheres within the animals. *F*, Fluorojade-positive cells were counted in a region of interest within the core of the lesion. Counts from both hemispheres were averaged for each slice. Data represent the mean ± S.E. from $n = 5$ (Nrf2$^{+/+}$), $n = 7$ (Nrf2$^{+/-}$), $n = 5$ (Nrf2$^{-/-}$). *, $p < 0.05$; **, $p < 0.01$; ***, $p < 0.001$, compared with wild-type control group, two-tailed *t* test.

cells have a well defined nuclear-cytoplasmic border.

Data Analysis—All data are shown as mean ± S.E. Statistical analyses were performed using Student's *t* test and one-way or two-way ANOVA in GraphPad Prism (version 2.01).

RESULTS

Nrf2$^{-/-}$ Mice Are Hypersensitive to Systemic 3-NP Treatment—Nrf2$^{-/-}$ mice were challenged with 3-NP to examine how loss of Nrf2 function affects both motor system impairment and toxicity attributed to metabolic inhibition *in vivo*. Our hypothesis was that Nrf2$^{-/-}$ mice would be more sensitive to the effects of 3-NP-induced metabolic inhibition. Thus, in initial experiments we determined *in vivo* 3-NP dosing regimes that would provide significant impairment in Nrf2$^{-/-}$ mice and then assessed what impact these had on wild-type animals. The extent of 3-NP toxicity was monitored through both manifestation of overt motor symptoms (*i.e.* reduced general locomotor activity, hind limb and truncal dystonia, and postural instability) and development of bilateral lesions restricted to the dorso-lateral striata (33). An advantage of using behavioral assessment as an adjunct to histology is that it can be performed repeatedly on the same animals providing a measure of 3-NP toxicity progression.

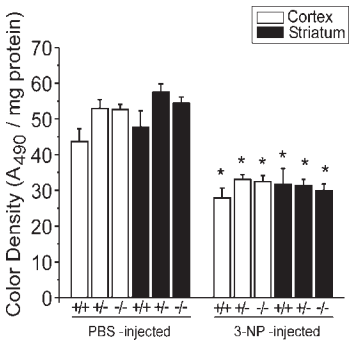

FIG. 2. **Inhibition of brain SDH is not different among Nrf2 genotypes 2 h after acute 3-NP injection.** Four mice from each genotype were injected with a single dose of 60 mg/kg 3-NP or PBS. 3-NP-injected mice were compared with PBS-injected littermates of the same genotype for each experiment. Animals were sacrificed 2 h after 3-NP injection when the peak of SDH inhibition has been shown to occur (47). Mitochondria samples were prepared from striatum and cortex and used in the SDH assay. A_{490} was normalized to mitochondrial protein content. Data represent the mean ± S.E. from $n = 4$ mice for each genotype and treatment group. *, $p < 0.05$, compared with PBS injected controls from same genotype, one-way ANOVA with Bonferroni post-hoc test.

TABLE I

Effects of Nrf2 genotype on basal and tBHQ-induced levels of antioxidant/detoxification markers in striatum, cortex, and liver

Basal phase 2 enzyme levels: GST, NQO1, and LDH activities from tissue extracts are expressed as nanomole/min/mg protein, and total GSH content is expressed as micrograms of GSH + GSSG/mg of protein. Data are represented as mean ± S.E. $n = 6$ animals, for both $Nrf2^{+/+}$ and $Nrf2^{-/-}$ groups. TBHQ-induced phase 2 enzyme levels: enzyme activities and GSH content were measured after 7 days of tBHQ feeding (1% w/w in mouse chow), and expressed as a percentage of values obtained from littermates with the same genotype receiving control diet. $n = 2$, 4, and 4 littermate pairs for $Nrf2^{+/+}$, $Nrf2^{+/-}$, and $Nrf2^{-/-}$ groups were used, respectively.

	Striatum		Cortex		Liver	
	+/+	−/−	+/+	−/−	+/+	−/−
Basal phase 2 enzyme levels						
GST	72.9 ± 6.9	57.4 ± 4.7[a]	65.9 ± 6.2	49.0 ± 4.9[b]	290.4 ± 35.8	195.0 ± 21.2[a]
NQO1	46.7 ± 1.3	37.3 ± 1.6[b]	29.7 ± 2.6	24.0 ± 1.2[c]	18.0 ± 4.0	5.2 ± 1.4[a]
GSH	28.5 ± 3.4	30.2 ± 4.8	23.1 ± 4.1	26.5 ± 3.9	110.5 ± 15.9	70.3 ± 9.3[c]
LDH	590.7 ± 49.6	601.5 ± 29.4	628.6 ± 27.9	686.8 ± 53.2	1094.6 ± 51.0	1234.7 ± 79.5
	+/+ and +/−	−/−	+/+ and +/−	−/−	+/+ and +/−	−/−
tBHQ-induced phase 2 enzyme levels (% control)						
GST	102.3 ± 3.5	107.9 ± 0.8	114.3 ± 9.1	126.4 ± 27.1	180.2 ± 13.4[d]	81.3 ± 21.7
NQO1	111.5 ± 9.3	109.1 ± 8.9	140.8 ± 22.6	117.8 ± 6.6	143.8 ± 8.2[d]	101.3 ± 12.0
GSH	126.8 ± 9.4[d]	107.1 ± 6.8	160 ± 19.8[d]	109.5 ± 14	117.0 ± 12.8	151.2 ± 13.9[d]
LDH	102.4 ± 2.5	95.9 ± 4.3	99.4 ± 4.7	106.4 ± 8.4	98.2 ± 3.4	100.0 ± 2.0

[a] $p < 0.01$, compared to wild-type littermates, two-tailed paired *t*-test.
[b] $p < 0.001$, compared to wild-type littermates, two-tailed paired *t*-test.
[c] $p < 0.05$, compared to wild-type littermates, two-tailed paired *t*-test.
[d] $p < 0.05$, compared to littermates fed control diet, two-tailed paired *t*-test.

In assays of motor behavior $Nrf2^{-/-}$ mice were indistinguishable from $Nrf2^{+/+}$ and $Nrf2^{+/-}$ controls before 3-NP treatment. However, with progressively increasing doses of 3-NP (given 12 h apart), $Nrf2^{-/-}$ mice exhibited motor deficits more quickly than controls (Fig. 1*A*). This increased sensitivity of $Nrf2^{-/-}$ mice became obvious after the 9th scheduled injection (60 mg/kg dose). 3-NP administration was ceased at this point because of increased morbidity of $Nrf2^{-/-}$ mice. Preceding motor deficits, $Nrf2^{-/-}$ mice also began to lose significant amounts of weight compared with control groups (Fig. 1*B*). By the end of the experiment, $Nrf2^{-/-}$ mice lost nearly 20% of their body weight. Consistent with behavioral scores, the doses given were insufficient to produce striatal lesions in $Nrf2^{+/+}$ mice. However, the majority of 3-NP challenged $Nrf2^{-/-}$ mice exhibited extensive striatal lesioning (Fig. 1, *C* and *D*, *left column*, and *E*). $Nrf2^{+/-}$ mice also developed striatal lesions that, on average, were ~7-fold smaller than in $Nrf2^{-/-}$ mice (lesion volumes, +/+ = 0.00 ± 0.00 mm^3, +/− = 0.74 ± 0.41 mm^3, −/− = 5.24 ± 1.50 mm^3, uncorrected for edema). Both motor deficits and weight loss were highly correlated with lesion size during 3-NP treatment (supplemental materials Fig. 1) (46). In addition, edema was likely contributing to the pathology of these mice because the striatal volume of 3-NP-treated $Nrf2^{-/-}$ mice was ~27% larger than controls (total striatal volume, +/+ = 7.95 ± 0.54 mm^3, +/− = 7.98 ± 0.29 mm^3, −/− = 10.14 ± 1.19 mm^3, *, $p < 0.05$).

Lesions of $Nrf2^{-/-}$ mice contained mainly pyknotic cells that stained positive for Fluorojade, a marker of neuronal degeneration (Fig. 1, *D*, *center* and *right column*s, and *F*) (34). Only a subpopulation of the remaining neurons in the $Nrf2^{+/-}$ lesions was Fluorojade-positive, and little or no positive cells were observed in the striata of $Nrf2^{+/+}$ mice. No significant extrastriatal (*i.e.* hippocampal or cortical) Fluorojade-positive staining was observed in 3-NP-treated $Nrf2^{-/-}$ mice, consistent with the striatal-specific action of systemic 3-NP administration. Importantly, $Nrf2^{-/-}$ mice were specifically sensitive to 3-NP because injection of PBS control solution caused negligible motor abnormalities and no lesions/Fluorojade-positive neurodegeneration (data not shown). Although the treatment regimen we used did not cause toxicity in $Nrf2^{+/+}$ mice, prolonged 3-NP administration (1–2 doses of 60 mg/kg 3-NP beyond current regimen) was able to provoke the development of motor deficits and lesions in this genotype (data not shown).

Striatal SDH Inhibition by 3-NP Is Not Different Among Genotypes—Because we used systemic administration of 3-NP, it was possible that increased toxicity in $Nrf2^{-/-}$ mice was because of compromised peripheral detoxification systems (*i.e.* liver, kidney, and intestines), leading to a higher circulating concentration of 3-NP in the brain. To address this possibility, we directly quantified SDH activity in the brain after an acute systemic injection of 3-NP (60 mg/kg). The cortex and striatum were collected after 2 h when peak brain SDH inhibition was shown to occur (47). SDH activity was reduced by 40–50% in total tissue from cortex and striatum of all genotypes, consistent with previous studies (Fig. 2) (47). Importantly, we observed no difference in SDH activity between genotypes, suggesting that increased damage caused by 3-NP in $Nrf2^{-/-}$ mice is most likely because of an intrinsic sensitivity in their brains.

Pre-activation of Nrf2 by tert-Butylhydroquinone Attenuates 3-NP Toxicity in $Nrf2^{+/-}$, but Not $Nrf2^{-/-}$ Mice—Nrf2 induction by small electrophilic molecules represents a practical method to increase the phase 2 response *in vivo* (48–50). Dietary administration of Nrf2 inducers, such as sulforaphane (isolated from broccoli sprouts) have been shown to induce phase 2 genes in peripheral tissues and reduce toxicity associated with a number of pathologies, including stomach tumor formation and hypertension (18, 51). To determine whether *in vivo* induction of Nrf2 could provide resistance to 3-NP toxicity, mouse diets were supplemented with the potent Nrf2 inducer, tBHQ (1, 52).

The *in vivo* phase 2 response was assessed by measuring the activities of two prototypic phase 2 enzymes, glutathione *S*-transferase (GST) and NAD(P)H:quinone oxidoreductase (NQO1), as well as total glutathione (GSH) content. $Nrf2^{-/-}$ mice exhibited lower basal striatal and cortical activity for GST and NQO1, when compared with $Nrf2^{+/+}$ littermate controls (Table I, basal phase 2 enzyme levels). Interestingly, basal brain GSH levels were not altered, suggesting that constitutive synthesis of brain GSH does not rely on Nrf2 function, at least in the young adult mice examined in here. As observed in previous studies, GST, NQO1 activities, and total GSH levels were markedly reduced in the livers of $Nrf2^{-/-}$ mice (53–56). The housekeeping gene, *ldh*, is not regulated by Nrf2 and accordingly, no significant differences in activity were observed between genotypes.

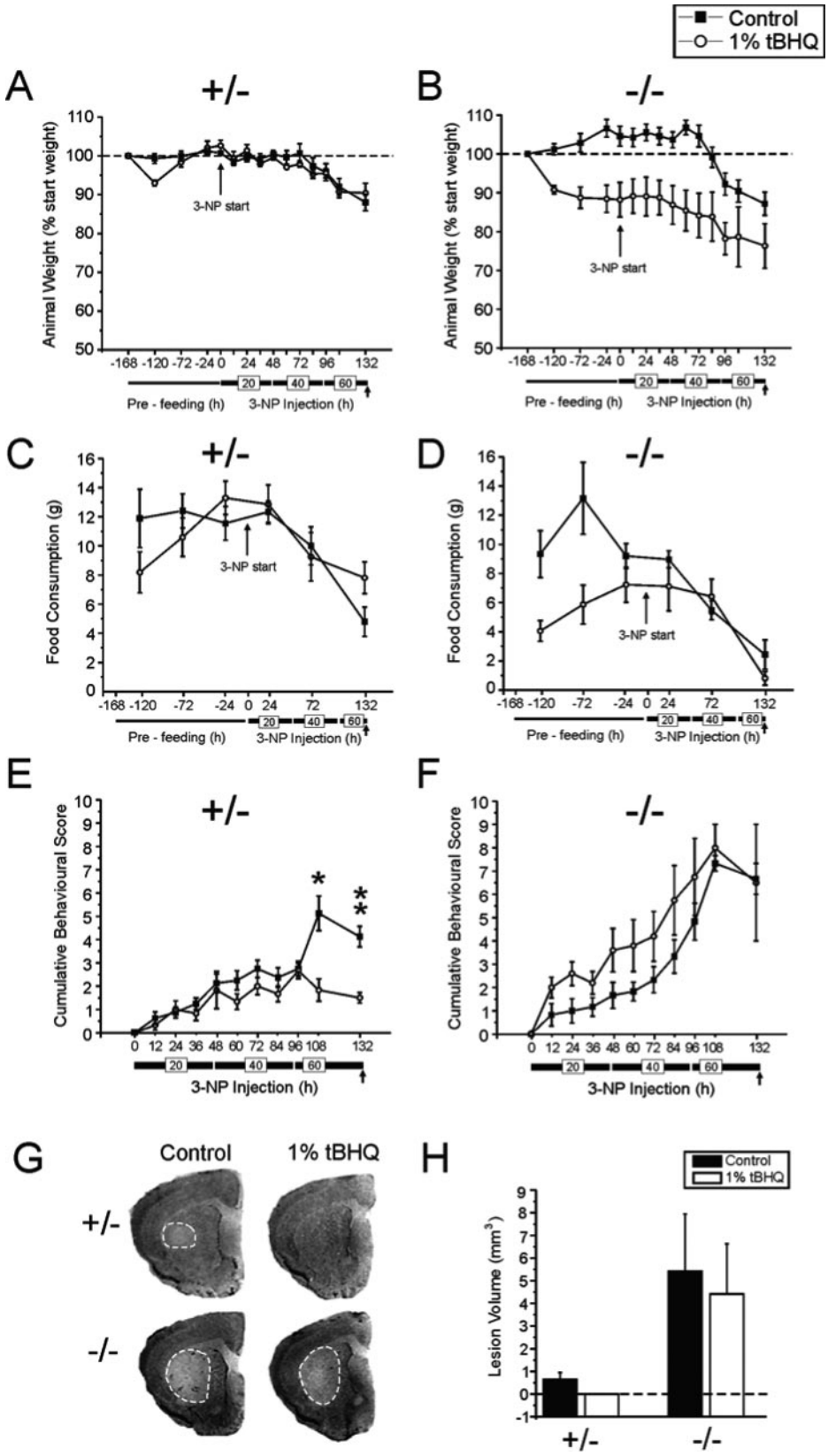

FIG. 3. **Dietary supplementation of tBHQ attenuates 3-NP toxicity in Nrf2$^{+/-}$ mice, but exacerbates toxicity in Nrf2$^{-/-}$ mice.** Mice received a tBHQ-supplemented diet for 1 week prior to and during 3-NP administration. Only Nrf2$^{+/-}$ and Nrf2$^{-/-}$ mice were studied because we were interested in observing reduced motor deficit and lesion size with tBHQ treatment, and Nrf2$^{+/+}$ mice did not develop these phenotypes. *A*, no significant differences were observed in body weight of Nrf2$^{+/-}$ mice between tBHQ and control diet. *B*, Nrf2$^{-/-}$ mice never fully adjusted to the tBHQ-supplemented diet where body weight of tBHQ-fed Nrf2$^{-/-}$ mice dropped by 10–20% during 1 week of feeding. *C*, control diet and tBHQ-fed Nrf2$^{+/-}$ mice consumed similar amounts of food throughout the experiment. *D*, Nrf2$^{-/-}$ mice consumed less food than Nrf2$^{-/-}$ mice with control diet. *E*, tBHQ-fed Nrf2$^{+/-}$ mice exhibited reduced motor deficit at the end of the 3-NP treatment regimen. *F*, an overall exacerbation of 3-NP-induced motor deficits was associated with tBHQ feeding of Nrf2$^{-/-}$ mice. *G* and *H*, tBHQ feeding prevented lesion development in Nrf2$^{+/-}$ mice, but had no effect on Nrf2$^{-/-}$ mice. Lesions are outlined by *dotted lines*. For the Nrf2$^{+/-}$ group, $n = 8$ and 6 animals were used for control and tBHQ-supplemented diets, respectively. For the Nrf2$^{-/-}$ group, $n = 6$ and 5 animals were used for control and tBHQ-supplemented diets, respectively. Data represents mean ± S.E. *, $p < 0.05$; **, $p < 0.01$, compared with Nrf2$^{+/-}$ mice receiving control diet, one-way ANOVA with Bonferroni post-hoc test.

Primarily Nrf2$^{+/-}$ and Nrf2$^{-/-}$ mice were used in tBHQ feeding studies because we were interested in observing reduced motor deficit and lesion size during 3-NP treatment, and Nrf2$^{+/+}$ mice did not develop these phenotypes. The tBHQ-supplemented diet (1% w/w) was well tolerated by Nrf2$^{+/-}$ mice because no significant weight loss was observed over 1 week of feeding, except a transient loss of weight 2 days after initiation of feeding, and food consumption was similar with mice receiving the control diet (Fig. 3, *A* and *C*). However, Nrf2$^{-/-}$ mice were less tolerant of dietary tBHQ with overall body weight ~10–20% lower than mice with control diet during 1 week of feeding (Fig. 3*B*, ***, $p < 0.0001$ two-way ANOVA), and less food consumption than tBHQ-fed Nrf2$^{+/-}$ mice (Fig. 3*D*). In total, Nrf2$^{+/-}$, and Nrf2$^{-/-}$ mice consumed 12.9 ± 0.9 and

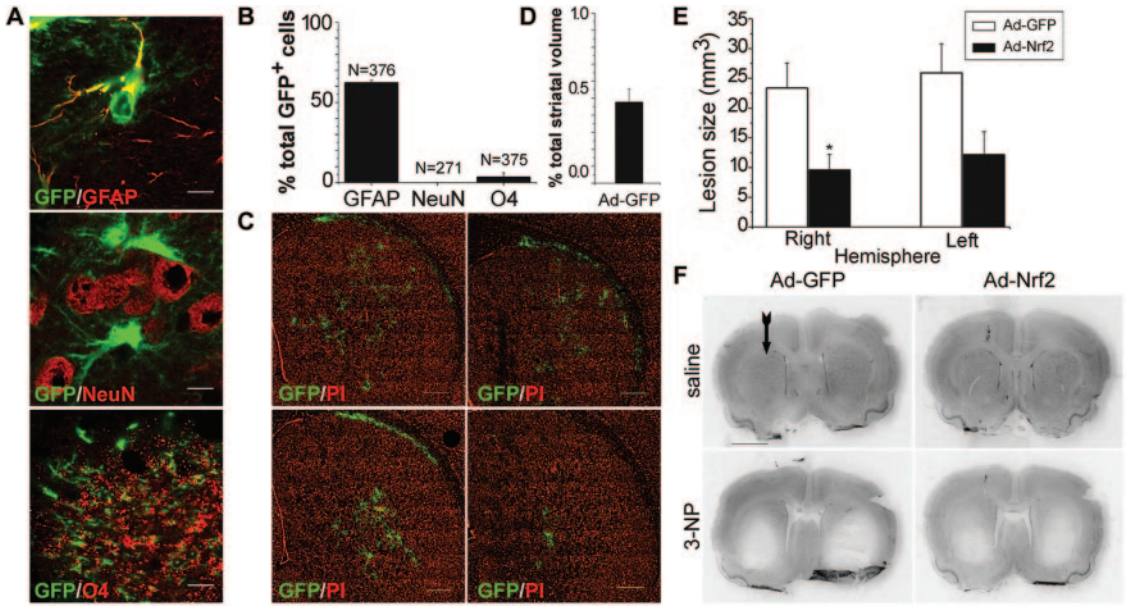

FIG. 4. **Ad-Nrf2 infected animals developed smaller lesions than Ad-GFP control animals following 3-NP administration.** *A*, immunostaining of GFP with the cell type-specific markers for astrocytes (GFAP, *top panel*), neurons (NeuN, *middle panel*), and oligodendrocytes (O4, *bottom panel*) was first performed to characterize the specificity of viral infection in rats *in vivo*. *Scale bars* = 10 μm. *B*, incidence of co-labeling between GFP and the different markers. *N* represents the total number of GFP$^+$ cells counted for two animals. *C*, representative images of GFP expression in the striatum of Ad-GFP-infected animals at Bregma (*clockwise* from *top left*) 1.00 mm, 0.48 mm, −0.80 mm, and −0.26 mm. *Scale bars*, 500 μm. *D*, analysis of GFP fluorescence as a percentage of total striatal volume (as determined by the area outlined by a propidium iodide counterstain, $n = 11$ animals). *E*, quantification of 3-NP-induced lesion volumes in the ipsilateral (*right*) and contralateral (*left*) hemispheres. Data represent mean ± S.E. of $n = 5$ animals per group. *, $p < 0.05$, compared with Ad-GFP infected controls, two-tailed *t* test. *F*, representative cresyl violet-stained sections at Bregma 0.70 mm for all the indicated treatment groups. *Arrow* indicates hemisphere receiving the adenoviral vector. *Scale bar* = 2.5 mm.

7.6 ± 0.7 mg of tBHQ/g of body weight over 1 week, respectively. The 1% tBHQ diet increased striatal and cortical GSH levels in Nrf2-expressing mice (Nrf2$^{+/+}$ and Nrf2$^{+/-}$) (Table I, tBHQ-induced phase 2 enzyme levels). Importantly, the induction of brain GSH was not observed in Nrf2$^{-/-}$ mice, providing evidence that tBHQ-induced changes in GSH are Nrf2 dependent. In addition, the tBHQ-induced increase in liver GST and NQO1 activities was observed in Nrf2 expressing mice, but not Nrf2$^{-/-}$ mice, consistent with the effects of other Nrf2 inducers used *in vivo* (56, 57). However, no induction of GST or NQO1 was detected in brain. Levels of the negative control enzyme, LDH, was unaffected by tBHQ in all tissues examined. Interestingly, we observed increased liver GSH levels in tBHQ-fed Nrf2$^{-/-}$ mice. We believe that this Nrf2-independent change may reflect an inherent hepatic toxicity associated with tBHQ feeding, perhaps because of inefficient detoxification from the body by the same pathways regulated by Nrf2 (phase 2 genes). Together, these results highlight the sensitivity of the Nrf2$^{-/-}$ phenotype to tBHQ toxicity and suggest normal phase 2 induction in response to tBHQ is abrogated in Nrf2$^{-/-}$ mice.

The tBHQ diet was given 1 week prior to the 3-NP regimen and maintained until sacrifice. TBHQ-fed Nrf2$^{+/-}$ mice had significantly attenuated 3-NP-induced motor deficits compared with mice receiving the control diet (Fig. 3*E*, **, $p <$ 0.001 two-way ANOVA). In contrast, tBHQ-fed Nrf2$^{-/-}$ mice exhibited an overall exacerbation of motor deficit (Fig. 3*F*, ***, $p = 0.0002$ two-way ANOVA). The average lesion volume of Nrf2$^{+/-}$ given control diet was similar to that measure in our initial experiments (0.65 + 0.29 mm^3, uncorrected for edema) (Fig. 3, *G* and *H*). However, consistent with reduced behavioral scores, no tBHQ-fed Nrf2$^{+/-}$ mice exhibited detectable lesions indicating protection of neurons. TBHQ feeding did not reduce lesion size in Nrf2$^{-/-}$ mice, confirming the protective effect of tBHQ consumption was Nrf2-dependent (Fig. 3, *G* and *H*).

Adenoviral Overexpression of Nrf2 Attenuates 3-NP-induced Striatal Lesioning in Vivo—To further address whether activation of Nrf2-dependent pathways is sufficient to protect the striatum during 3-NP toxicity, in parallel studies, we tested whether direct Nrf2 overexpression using adenovirus vectors (Ad-Nrf2 or Ad-GFP control) conferred neuroprotection to rats treated with 3-NP. Overexpression of Nrf2 causes its accumulation in the nucleus leading to even more robust ARE-dependent transcription than that observed with small molecule inducer treatment (43). *In vivo* intrastriatal adenovirus injection primarily led to infection of astrocytes (Fig, 4, *A*, *top panel*, and *B*), and almost no neurons or oligodendrocytes (Fig. 4*A*, *middle* and *bottom panel*, and *B*). Vector diffusion was observed throughout the striatum (Fig. 4*C*), infecting 0.48 ± 0.08% of the total striatal volume, as assessed by the presence of the GFP marker (Fig. 4*D*). After infection, protein expression was allowed to occur for 3 days before 3-NP treatment was initiated.

Following 3-NP challenge, lesion volumes in the infected hemisphere were significantly smaller in animals receiving Ad-Nrf2, compared with Ad-GFP control virus (9.6 ± 2.6 mm^3 *versus* 23.4 ± 4.2 mm^3, $p = 0.03$, two-tailed *t* test, Fig. 4, *E* and *F*). Interestingly, a trend toward decreased lesion volume was also observed in the hemisphere contralateral to the virus injection (12.2 ± 3.8 mm^3 compared with 25.9 ± 4.9 mm^3, $p =$ 0.06), although this difference did not attain statistical significance. This effect may be because of diffusion of secreted glial factors, possibly glutathione or glutathione precursors, by volume transmission along fiber bundles of the corpus callosum, or through the cerebral spinal fluid from the infected Nrf2 overexpressing astrocytes in the ipsilateral hemisphere (58, 59).

3-NP Activates ARE-dependent Gene Expression in Cultured Astrocytes—Our data show that both the Nrf2 inducer tBHQ and Nrf2 overexpression can protect neurons by pre-activating the phase 2 response. Because increased susceptibility of Nrf2$^{-/-}$ mice may result from the inability to activate expres-

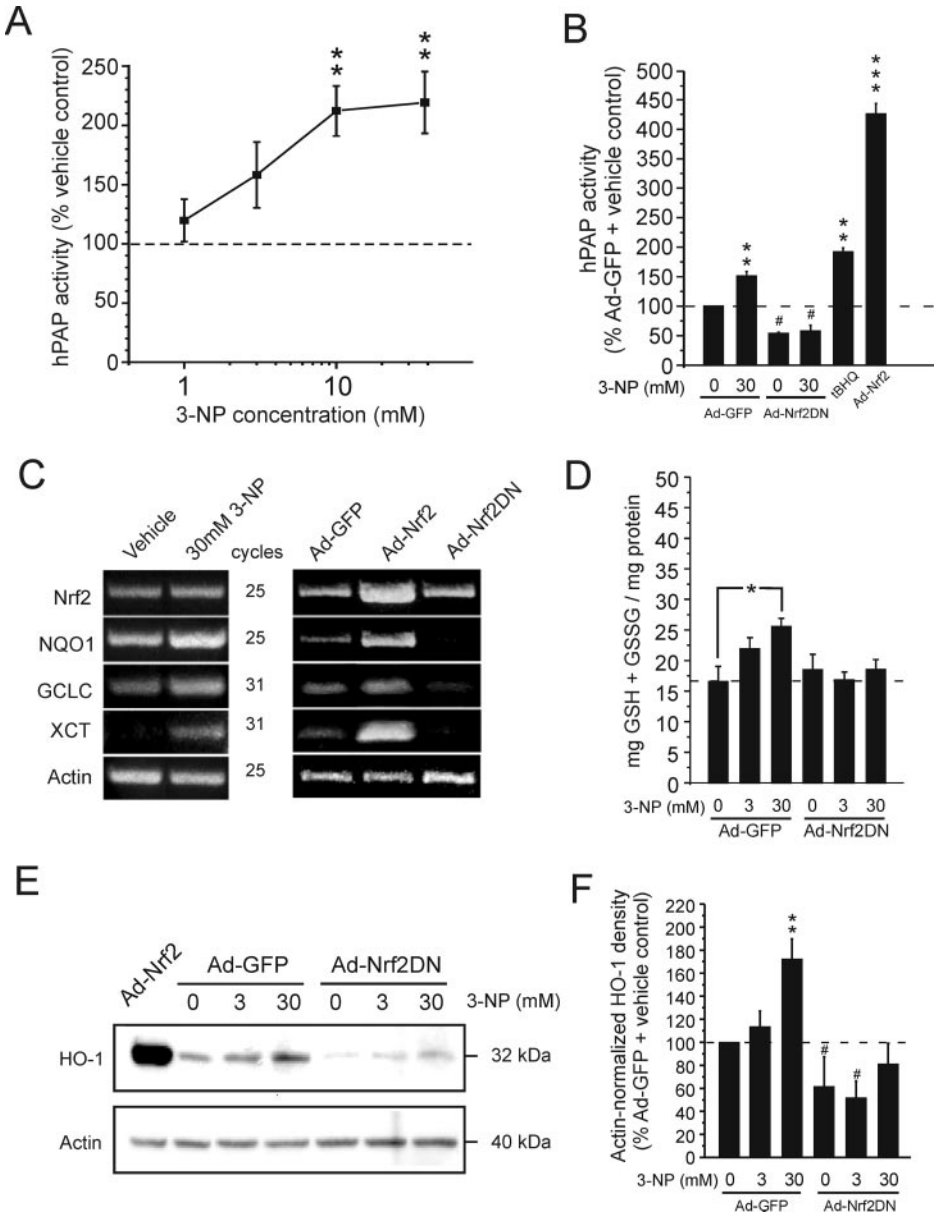

FIG. 5. **3-NP exposure induces ARE-dependent gene expression in cultured astrocytes.** *A*, cultured cortical astrocytes were transiently transfected with a hPAP reporter construct regulated by an ARE-bearing *nqo1* promoter (41). The astrocytes were then treated with varying concentrations of 3-NP (1–30 mM) for 2 h in a glucose-free basic salt solution (*BSS vehicle*), followed by washout. A doubling of hPAP activity was observed 24 h after 10 or 30 mM 3-NP treatment. *B*, expression of ARE-driven hPAP, with vehicle or 3-NP exposure, was reduced to sub-basal levels when astrocytes overexpressed a dominant-negative form of Nrf2 (Ad-Nrf2DN), but not with overexpression of a GFP control (Ad-GFP) (6). ARE-driven hPAP was induced by 24 h of tBHQ exposure and maximally increased with Ad-Nrf2 infection. Data represent the mean ± S.E. from three independent experiments. *C*, semi-quantitative RT-PCR confirmed that astrocytes treated with 30 mM 3-NP expressed more mRNAs from prototypic Nrf2 target genes including *nqo1*, *gclc*, and *Xct*. DNA templates were serially diluted to ensure that band intensities were observed within the linear range of the PCR (supplemental materials Fig. 2). As controls, Ad-Nrf2- and Ad-Nrf2DN-infected cultures were also evaluated with RT-PCR. In all cases, the mRNA levels were induced with Nrf2 overexpression and suppressed with Nrf2DN overexpression. RT-PCR experiments were reproduced three times with similar results. *D*, cultures treated with 30 mM 3-NP produced more total intracellular GSH than vehicle treated controls. GSH induction was blocked with Ad-Nrf2DN infection, but not Ad-GFP control. *E*, Western blot analysis shows that protein expression of HO-1 was induced with 30 mM 3-NP treatment in Ad-GFP-infected cultures. Both basal and induced expression of HO-1 was largely blocked with Ad-Nrf2DN infection. *F*, densitometric analyses of HO-1 protein levels. GSH and HO-1 data represent the mean ± S.E. from three independent experiments. *, $p < 0.05$; **, $p < 0.01$; ***, $p < 0.001$, two-tailed paired *t* test.

sion of protective genes necessary for reducing toxicity associated with 3-NP, we hypothesized that metabolic inhibition by 3-NP was acting as a signal for Nrf2 activation. To test this hypothesis, we examined the effect of 3-NP on Nrf2 activity in cultured astrocytes, the primary site of ARE-mediated gene expression in brain cultures (6, 41, 60).

To mimic the effects of bolus *in vivo* injection, cultured astrocytes were treated with a wide range of 3-NP concentrations (1–30 mM) for 2 h and then ARE-mediated gene expression was assessed 24 h later using a hPAP reporter assay regulated by an ARE-bearing *nqo1* promoter (Fig. 5*A*) (41). Astrocytes transiently treated (2 h) with 10–30 mM 3-NP exhibited a doubling of ARE-mediated gene expression. Over these time periods and with these 3-NP concentrations no apparent astrocyte toxicity was observed. Expression of ARE-driven hPAP, with and without 3-NP exposure, was reduced to sub-basal levels when astrocytes were infected with adenovirus overexpressing a dominant-negative form of Nrf2 (Ad-Nrf2DN), but not with overexpression of GFP control (Ad-GFP) (Fig. 5*B*) (6). Exposure to tBHQ (20 μM for 24 h) induced hPAP expression to a simi-

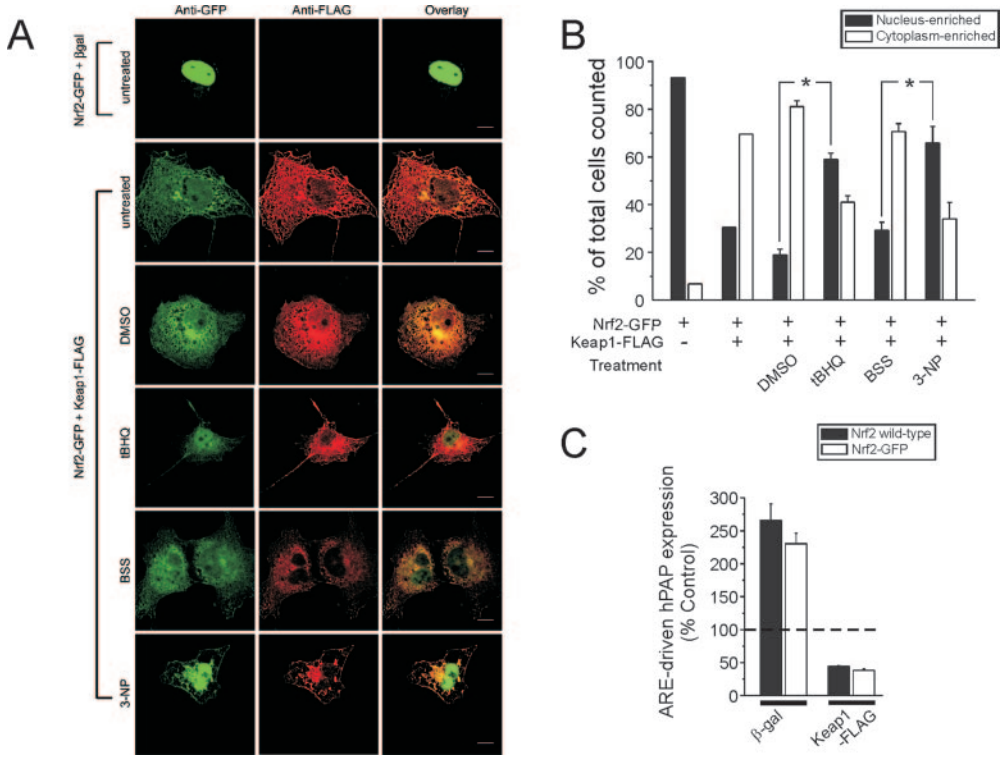

FIG. 6. **3-NP promotes nuclear translocation of Nrf2-GFP.** *A*, COS-1 cells were transiently transfected with Nrf2-GFP (N-terminal fusion to Nrf2) with and without Keap1-FLAG. Consistent with previous studies, overexpressed Nrf2-GFP was almost exclusively localized to the nucleus unless co-expressed with its cytoplasmic regulator Keap1 (*top row*) (13, 43). COS-1 cells co-expressing Nrf2-GFP and Keap1-FLAG were evaluated after treatment with 3-NP or BSS vehicle control. The proportion of cells exhibiting nuclear-enriched Nrf2-GFP was significantly higher in 3-NP-treated cultures, when compared with vehicle control. 3-NP also appeared to cause a transient aggregation of some Keap1-FLAG and Nrf2-GFP in the cytoplasm (*bottom row*). Treatment with 20 μM tBHQ for 4 h, as a positive control, also robustly increased nuclear localization of Nrf2-GFP (*scale bar* = 10 μm). *B*, summary of Nrf2-GFP localization in response to tBHQ and 3-NP. *C*, both Nrf2-GFP and Keap1-FLAG constructs were functional, as assessed by their ability to augment and suppress ARE-driven hPAP expression, respectively. Data represents three separate experiments scored by a researcher blinded to the treatment conditions (total cells evaluated: $n = 119$ and $n = 158$, BSS and 3-NP-treated cells, respectively). *, $p < 0.05$, two-tailed paired t test.

lar extent as 3-NP treatment. Maximal hPAP activity was achieved with Nrf2 overexpression (Ad-Nrf2). Although the concentrations of 3-NP we used to activate Nrf2 mediated gene expression were high, the ability of dominant negative Nrf2 to block the induction indicates that it is nonetheless mediated by the ARE. Perhaps these high concentrations reflect the activated and toxin-resistant nature of astrocytes *in vitro* (61).

Semi-quantitative RT-PCR confirmed that astrocytes treated with 30 mM 3-NP for 2 h expressed higher levels of prototypic Nrf2 target gene mRNAs including *nqo1*, γ-glutamylcysteine synthetase (*gclc*), and the cystine/glutamate exchanger (*Xct*) (Fig. 5*C*). The expression of these mRNAs was increased by Ad-Nrf2 and suppressed by Ad-Nrf2DN infection, verifying the specificity of these target genes. For all RT-PCR experiments, DNA templates were serially diluted to ensure that band intensities were observed within the linear range of the PCR (supplemental materials Fig. 2). Because a number of Nrf2 target genes are involved in GSH synthesis (*i.e. Xct*, *gclc*, and glutathione synthase), treatment with 30 mM 3-NP also increased intracellular GSH levels in cultured astrocytes (Fig. 5*D*) (5, 6, 54, 55). Consistent with ARE-driven hPAP expression, 3-NP-mediated GSH induction was blocked with Ad-Nrf2DN infection, but not Ad-GFP control (Fig. 5*D*). Protein levels of heme oxygenase-1 (HO-1), a well characterized Nrf2 target, were also induced by 3-NP treatment (Fig. 5, *E* and *F*) (1). Both basal and induced expression of HO-1 was suppressed with Ad-Nrf2DN infection. Although this analysis does not encompass the full scope of Nrf2 gene targets, it nevertheless indicates the phase 2 response is activated as a dose-dependent effect of 3-NP.

We further evaluated nuclear translocation of GFP-tagged Nrf2 (Nrf2-GFP) in response to 3-NP exposure. In initial experiments using astrocytes, Nrf2-GFP fluorescence was almost undetectable when co-expressed with its cytoplasmic regulator Keap1, possibly because of a faster rate of Nrf2 turnover by proteasome-dependent pathways (62). As an alternative, COS-1 cells were used because of their high level of transgene expression and well defined morphology for evaluating nuclear *versus* cytoplasmic localization. Consistent with previous studies, overexpressed Nrf2-GFP was almost exclusively localized to the nucleus unless co-expressed with Keap1 (Keap1-FLAG) (Fig. 6*A*, *top row*) (13, 43). COS-1 cells co-expressing Nrf2-GFP and Keap1-FLAG were evaluated after treatment with 3-NP or BSS vehicle control for 2 h. As expected, the proportion of cells exhibiting nucleus-enriched Nrf2-GFP fluorescence was significantly higher in 3-NP-treated cultures, when compared with vehicle control (Fig. 6, *A* and *B*). Interestingly, 3-NP treatment also caused some aggregation of Keap1 and Nrf2-GFP in the cytoplasm, which we speculate is because of 3-NP-induced endoplasmic reticulum stress causing accumulation of unfolded proteins (63). This effect was transient because the aggregations were not observed 24 h after 3-NP washout (data not shown). Treatment with 20 μM tBHQ for 4 h, as a positive control, also robustly increased nuclear localization of Nrf2-GFP (Fig. 6, *A* and *B*). Both Nrf2-GFP and Keap1-FLAG constructs were functional, as assessed by their ability to augment and suppress ARE-driven hPAP expression, respectively (Fig. 6*C*).

Collectively, this *in vitro* data confirms Nrf2 translocates to the nucleus and initiates phase 2 gene induction in response to 3-NP-mediated metabolic inhibition. This effect can be mim-

icked using the Nrf2 inducer, tBHQ, and by adenoviral Nrf2 overexpression.

DISCUSSION

This study provides evidence to support the neuroprotective function of Nrf2 during metabolic compromise in the *in vivo* brain. First, loss of Nrf2 function led to an increased susceptibility to 3-NP because $Nrf2^{-/-}$ mice developed motor deficits and striatal lesions more rapidly than Nrf2 expressing controls. Second, pre-activation of endogenous Nrf2 using the small molecule inducer, tBHQ, attenuated 3-NP toxicity in $Nrf2^{+/-}$ mice, but not $Nrf2^{-/-}$, confirming both the neuroprotective action and Nrf2 dependence of tBHQ *in vivo*. Third, direct overexpression of Nrf2 in the striatum is sufficient to reduce lesion size caused by 3-NP. Fourth, ARE-dependent gene expression in cultured astrocytes was activated by 3-NP, and could be completely suppressed by overexpression of a dominant-negative form of Nrf2.

$Nrf2^{-/-}$ Mice Are Hypersensitive to 3-NP Toxicity—The increased sensitivity of $Nrf2^{-/-}$ mice may result from an inability to induce phase 2 genes in response to 3-NP toxicity. Indeed, a recent study by Calkins *et al.* (64) (published while this work was submitted) showed using transgenic reporter mice, that ARE-dependent gene expression occurred in the immediate border of 3-NP induced striatal lesions, perhaps in reactive astrocytes commonly found within this region (64). Because Nrf2 is generally thought to respond to oxidative stress or signal transduction pathways associated with it (65, 66), we speculate that 3-NP activates this protective pathway by indirectly generating ROS/RNS. 3-NP may increase brain oxidative stress through multiple mechanisms that may be implicated in our *in vitro* and *in vivo* experiments (6, 27, 29, 30). Also supported by our data, an alternative possibility for the increased sensitivity of $Nrf2^{-/-}$ mice may be the lower basal levels of phase 2 enzymes expressed in this genotype (Table I, basal phase 2 enzyme levels) (83).

Given that systemic 3-NP undergoes first pass metabolism before it reaches the striatum, it was possible that increased striatal damage in $Nrf2^{-/-}$ mice was in part because of impaired clearance of 3-NP from the body by peripheral detoxification. Indeed previous studies of $Nrf2^{-/-}$ mice have shown decreased phase 2 enzyme activity in the liver and intestines (53, 67), organs that may affect the removal of systemically injected 3-NP. However, we have shown that after a single high *in vivo* dose of 3-NP, striatal SDH was inhibited to an equal extent between $Nrf2^{+/+}$ and $Nrf2^{-/-}$ genotypes, suggesting that 3-NP produces similar metabolic inhibition on a dose-wise basis regardless of genotype. Thus, it appears that the brains of $Nrf2^{-/-}$ mice are intrinsically more sensitive to direct damage. This conclusion is also supported by a number of other findings. First, neurons and glia isolated from $Nrf2^{-/-}$ mice are more sensitive to *in vitro* toxicity paradigms involving oxidative stress or metabolic compromise (8, 27, 28). Second, direct injection of malonate (reversible SDH inhibitor) into the striatum produced larger lesions in $Nrf2^{-/-}$ mice, compared with Nrf2 expressing controls (64). Third, $Nrf2^{-/-}$ mice develop larger cortical infarcts than $Nrf2^{+/+}$ mice after experimental stroke (permanent distal middle cerebral artery occlusion), a model that also involves local brain metabolic inhibition (31).[2]

The Small Molecule Inducer, tBHQ, Provided Nrf2-dependent Amelioration of 3-NP Toxicity in Vivo—Although studies indicate that loss of Nrf2 potentiates neurotoxicity (64), whether the *in vivo* neuroprotective effects of small molecule inducers are lost in Nrf2 knock-out mice has not been previously addressed. Recent *in vitro* studies have shown that tBHQ treatment augments ARE-dependent gene expression in cultured astrocytes and protects neurons from toxicity paradigms involving oxidative stress (6, 28, 68, 69). We extend these findings to the *in vivo* situation because dietary consumption of tBHQ significantly reduced motor deficits and lesion developments in $Nrf2^{+/-}$ mice. Importantly, the protective effect of tBHQ was abrogated in $Nrf2^{-/-}$ mice. Furthermore, dietary tBHQ administration increased brain GSH levels in $Nrf2^{+/+}$ and $Nrf2^{+/-}$ mice, but not $Nrf2^{-/-}$ mice (Table I, tBHQ-induced phase 2 enzyme levels).

As expected from previous studies (70), dietary tBHQ treatment also increased phase 2 enzyme activity (GST and NQO1) in the liver. Thus, it remains possible that attenuation of 3-NP toxicity in tBHQ-fed mice could be in part because of enhanced removal of 3-NP from the body by increased liver detoxification or conceivably liver-derived antioxidants such as GSH released into the blood. However, our observed increase in brain GSH would be expected to contribute to local neutralization of ROS/RNS, leading to tissue preservation. In preliminary studies, we have found that even local infusion of tBHQ in brain ventricles using osmotic pumps can lead to increases in liver phase 2 enzyme levels suggesting that it is difficult to completely dissociate brain and peripheral organ detoxification. Future studies could more directly address the role of brain Nrf2 by developing tissue and organ-specific Nrf2 knock-outs. However, in support of the brain being the site of tBHQ action, overexpression of Nrf2 within the striatum using adenovirus was sufficient to reduce the effect of systemically administered 3-NP. Although some uncertainty remains as to the site of Nrf2 induction mediated by tBHQ *in vivo*, our study nonetheless indicates that striatal-specific damage because of the systemic administration of a metabolic stressor can be strongly attenuated by this dietary strategy. Given that many neurodegenerative diseases may be triggered by exposure to diet or lung-derived toxins (71–73), it is conceivable that a dietary strategy to increase antioxidant function in multiple organs may be an ideal prophylactic strategy. To our knowledge, this is the first study to show that a protective effect of a phase 2 inducer on brain function *in vivo* is dependent on Nrf2.

Although tBHQ is widely used as a food antioxidant, and is well tolerated by the body (74, 75), it is also important to consider the detrimental action of tBHQ and other Nrf2 inducers. As observed in this study, $Nrf2^{-/-}$ mice do not tolerate tBHQ administration as well as controls (as evidenced by weight loss and reduced food consumption) perhaps because of inefficient detoxification of tBHQ through Nrf2-regulated pathways (Fig. 3, *A* and *B*). Other groups have also found that $Nrf2^{-/-}$ mice are less tolerant to dietary administration of known Nrf2 inducers (67). Recently, increased susceptibility to hypoxia has been linked to polymorphisms in the *Nrf2* gene (76). The question arises as to whether such mutations affect Nrf2 function in humans, and could underlie sensitivity to human disease. Because many Nrf2 inducers are essentially reactive electrophiles, the inability to properly detoxify Nrf2 inducers from the body could be harmful to individuals with such a genetic predisposition.

With regard to practical application, recent studies have elucidated a variety of structurally related small molecules that are able to activate Nrf2 by reacting with thiol/disulfide groups on the cytoplasmic regulatory protein Keap1 (4, 48, 50, 77–79). Some of these inducers are found within our diet. For example, the isothiocyanate sulforaphane, a potent Nrf2 inducer abundant in cruciferous plants (*i.e.* broccoli sprouts), was found to inhibit gastric tumor formation induced benzo[*a*]pyrene (78). Juurlink and colleagues (51, 80) have recently demonstrated a significant improvement of cardiovascular fit-

[2] A. Y. Shih and T. H. Murphy, unpublished data.

ness in spontaneously hypertensive rats through chronic upregulation of phase 2 enzymes by supplementing diets with broccoli sprouts. Such studies support the potential for mitigating oxidative tissue damage in chronic disorders involving oxidative stress, by applying a change in diet, a practical and realistic therapeutic approach from a clinical standpoint.

Overexpression of Nrf2 Protein Is Sufficient to Provide Neuroprotection in Vivo—We have also conducted a proof of principle experiment showing that adenoviral overexpression of Nrf2 in the striatum is sufficient to reduce 3-NP toxicity *in vivo*. Adenovirus was found to mainly infect astrocytes throughout the striatum as well as in the corpus callosum. In our immunohistochemical analysis, we observed that some GFP-positive cells with astrocyte morphology (~35%) were not labeled by any cell-type marker tested. However, these cells were labeled by a different astrocyte marker, S100β (total GFP and S100β co-localization = 91.8 + 0.2%, $n = 2$), confirming their identity (81). With regard to the extent of neuroprotection achieved with Nrf2 overexpression *in vivo*, we have previously demonstrated that a small number of Ad-Nrf2-infected astrocytes can confer protection to many neighboring neurons during an oxidative glutamate insult *in vitro* (1 astrocyte can protect 100 neurons) (6). These Nrf2 overexpressing astrocytes secrete high levels of glutathione, providing a means for a small number of astrocytes to affect the survival of a much larger number of neurons (6). In support of our findings, Calkins *et al.* (64) observed significant neuroprotection *in vivo* by transplanting a relatively small number of Nrf2 overexpressing astrocytes (from culture) directly into the striatum prior to injection of the competitive complex II inhibitor, malonate. In addition, many factors contributing to oxidative stress (*i.e.* ROS/RNS) are cell permeable allowing them to be metabolized in a subpopulation of cells (82). Another factor to consider is the actual spatial localization of the astrocytes infected *in situ*. The patchy nature of the infection (Fig. 4*C*) suggests a wider area can be protected within the volume of the brain. Furthermore, there is precedent for a small number of cells playing a major role in striatal function. One such example are the cholinergic interneurons of the striatum that only make up 1–2% of all striatal neurons yet have profound impact on the functional output of the striatum influencing such diverse behaviors as sensorimotor function, sleep and arousal states, learning and memory, anxiety, and pain sensations (83).

3-NP Exposure Activated ARE-mediated Gene Expression in Vitro—Our *in vitro* experiments show that 3-NP exposure upregulated phase 2 gene expression in cultured astrocytes, providing a mechanistic link between 3-NP and Nrf2 activation. The effect of 3-NP was attributed to Nrf2 because a dominant negative version of Nrf2 was able to block the effect of 3-NP. However, further experiments are necessary to determine which component of 3-NP toxicity acts as a signal for Nrf2 activation. For example, Nrf2 activation may result from 3-NP-induced ROS/RNS generation, loss of ATP, or even as a direct response to SDH inhibition. In preliminary studies using cultured astrocytes, we examined the level of SDH inhibition caused by the range of 3-NP concentrations used *in vitro*. After 2 h of exposure to non-Nrf2 inducing 3-NP concentrations (0.3–1 mM), SDH activity was reduced by ~90%. However, at Nrf2 inducing concentrations (10–30 mM), SDH activity was almost completely inhibited (~98%). Given this difference, it is possible that a non-linear relationship exists between SDH activity and activation of ARE-mediated gene expression. Conceivably, the requirement for high concentrations of 3-NP to induce Nrf2-mediated gene expression may in part be due to the high intrinsic resistance of cultured astrocytes that show an activated phenotype to agents that induce metabolic inhibition and oxidative stress (61).

CONCLUSION

Nrf2 plays an important role in regulating neuronal survival during metabolic compromise *in vivo*. The absence of Nrf2 function in Nrf2$^{-/-}$ mice exacerbates neurodegeneration caused by 3-NP administration. Augmentation of ARE-mediated gene expression in Nrf2-expressing animals using the small molecule inducer, tBHQ, attenuated tissue damage and preserved motor function. Dietary administration of Nrf2 inducers may have profound effects for neuronal viability in neurodegenerative disease, stroke, and related forms of energy deprivation.

Acknowledgments—We thank Dr. Yuet Wai Kan for Nrf2$^{-/-}$ mouse production, and Dr. Jeff Johnson for distributing the mice. We also thank the University of British Columbia Animal Care Facility, and Steve Callaghan at the University of Ottawa for production of adenoviruses, and Dr. Alaa El-Husseini for access to the Zeiss Meta confocal microscope.

REFERENCES

1. Alam, J., Stewart, D., Touchard, C., Boinapally, S., Choi, A. M., and Cook, J. L. (1999) *J. Biol. Chem.* **274,** 26071–26078
2. Itoh, K., Chiba, T., Takahashi, S., Ishii, T., Igarashi, K., Katoh, Y., Oyake, T., Hayashi, N., Satoh, K., Hatayama, I., Yamamoto, M., and Nabeshima, Y. (1997) *Biochem. Biophys. Res. Commun.* **236,** 313–322
3. Rushmore, T. H., Morton, M. R., and Pickett, C. B. (1991) *J. Biol. Chem.* **266,** 11632–11639
4. Talalay, P. (2000) *Biofactors* **12,** 5–11
5. Ishii, T., Itoh, K., Takahashi, S., Sato, H., Yanagawa, T., Katoh, Y., Bannai, S., and Yamamoto, M. (2000) *J. Biol. Chem.* **275,** 16023–16029
6. Shih, A. Y., Johnson, D. A., Wong, G., Kraft, A. D., Jiang, L., Erb, H., Johnson, J. A., and Murphy, T. H. (2003) *J. Neurosci.* **23,** 3394–3406
7. Thimmulappa, R. K., Mai, K. H., Srisuma, S., Kensler, T. W., Yamamoto, M., and Biswal, S. (2002) *Cancer Res.* **62,** 5196–5203
8. Lee, J. M., Calkins, M. J., Chan, K., Kan, Y. W., and Johnson, J. A. (2003) *J. Biol. Chem.* **278,** 12029–12038
9. Itoh, K., Wakabayashi, N., Katoh, Y., Ishii, T., Igarashi, K., Engel, J. D., and Yamamoto, M. (1999) *Genes Dev.* **13,** 76–86
10. Kang, M. I., Kobayashi, A., Wakabayashi, N., Kim, S. G., and Yamamoto, M. (2004) *Proc. Natl. Acad. Sci. U. S. A.* **101,** 2046–2051
11. Wakabayashi, N., Dinkova-Kostova, A. T., Holtzclaw, W. D., Kang, M. I., Kobayashi, A., Yamamoto, M., Kensler, T. W., and Talalay, P. (2004) *Proc. Natl. Acad. Sci. U. S. A.* **101,** 2040–2045
12. Dinkova-Kostova, A. T., Holtzclaw, W. D., Cole, R. N., Itoh, K., Wakabayashi, N., Katoh, Y., Yamamoto, M., and Talalay, P. (2002) *Proc. Natl. Acad. Sci. U. S. A.* **99,** 11908–11913
13. Itoh, K., Wakabayashi, N., Katoh, Y., Ishii, T., O'Connor, T., and Yamamoto, M. (2003) *Genes Cells* **8,** 379–391
14. Chan, K., Han, X. D., and Kan, Y. W. (2001) *Proc. Natl. Acad. Sci. U. S. A.* **98,** 4611–4616
15. Enomoto, A., Itoh, K., Nagayoshi, E., Haruta, J., Kimura, T., O'Connor, T., Harada, T., and Yamamoto, M. (2001) *Toxicol. Sci.* **59,** 169–177
16. Chan, K., and Kan, Y. W. (1999) *Proc. Natl. Acad. Sci. U. S. A.* **96,** 12731–12736
17. Cho, H. Y., Jedlicka, A. E., Reddy, S. P., Kensler, T. W., Yamamoto, M., Zhang, L. Y., and Kleeberger, S. R. (2002) *Am. J. Respir. Cell Mol. Biol.* **26,** 175–182
18. Fahey, J. W., Haristoy, X., Dolan, P. M., Kensler, T. W., Scholtus, I., Stephenson, K. K., Talalay, P., and Lozniewski, A. (2002) *Proc. Natl. Acad. Sci. U. S. A.* **99,** 7610–7615
19. Ramos-Gomez, M. C., Kwak, M. K., Dolan, P. M., Itoh, K., Yamamoto, M., Talalay, P., and Kensler, T. W. (2001) *Proc. Natl. Acad. Sci. U. S. A.* **98,** 3410–3415
20. Coyle, J. T., and Puttfarcken, P. (1993) *Science* **262,** 689–695
21. Beal, M. F., Brouillet, E., Jenkins, B. G., Ferrante, R. J., Kowall, N. W., Miller, J. M., Storey, E., Srivastava, R., Rosen, B. R., and Hyman, B. T. (1993) *J. Neurosci.* **13,** 4181–4192
22. Reynolds, I. J., and Hastings, T. G. (1995) *J. Neurosci.* **15,** 3318–3327
23. Schulz, J. B., Matthews, R. T., Jenkins, B. G., Ferrante, R. J., Siwek, D., Henshaw, D. R., Cipolloni, P. B., Mecocci, P., Kowall, N. W., Rosen, B. R., and Beal, M. F. (1995) *J. Neurosci.* **15,** 8419–8429
24. Beal, M. F. (1995) *Ann. Neurol.* **38,** 357–366
25. Beal, M. F. (1992) *Ann. Neurol.* **31,** 119–130
26. Reynolds, D. S., Carter, R. J., and Morton, A. J. (1998) *J. Neurosci.* **18,** 10116–10127
27. Lee, J. M., Shih, A. Y., Murphy, T. H., and Johnson, J. A. (2003) *J. Biol. Chem.* **278,** 37948–37956
28. Kraft, A. D., Johnson, D. A., and Johnson, J. A. (2004) *J. Neurosci.* **24,** 1101–1112
29. Duffy, S., So, A., and Murphy, T. H. (1998) *J. Neurochem.* **71,** 69–77
30. Murphy, T. H., De Long, M. J., and Coyle, J. T. (1991) *J. Neurochem.* **56,** 990–995
31. Shih, A. Y., Li, P., Earl, N., Imbeault, S., Cheng, M. N., Gilbert, R., Robertson, G. S., and Murphy, T. H. (2004) *2004 Abstract Viewer/Itinerary Planner*, Program No. 456.13, Society for Neuroscience, Washington, D. C., online

32. Chan, K., Lu, R., Chang, J. C., and Kan, Y. W. (1996) *Proc. Natl. Acad. Sci. U. S. A.* **93,** 13943–13948
33. Fernagut, P. O., Hervier, L., Labattu, B., Bioulac, B., and Tison, F. (2002) *Neuroscience* **115,** 533–546
34. Schmued, L. C., Albertson, C., and Slikker, W., Jr. (1997) *Brain Res.* **751,** 37–46
35. Paxinos, G., and Franklin, K. B. J. (2001) *The Mouse Brain in Stereotaxic Coordinates*, 2nd Ed., Academic Press, San Diego
36. Paxinos, G., and Watson, C. (1986) *The Rat Brain in Stereotaxic Coordinates*, 2nd Ed., Academic Press, Sydney
37. Pennington, R. J. (1961) *Biochem. J.* **80,** 649–654
38. Benson, A. M., Hunkeler, M. J., and Talalay, P. (1980) *Proc. Natl. Acad. Sci. U. S. A.* **77,** 5216–5220
39. Kelly, V. P., Ellis, E. M., Manson, M. M., Chanas, S. A., Moffat, G. J., McLeod, R., Judah, D. J., Neal, G. E., and Hayes, J. D. (2000) *Cancer Res.* **60,** 957–969
40. Everse, J., Berger, R. L., and Kaplan, N. O. (1970) *Science* **168,** 1236–1238
41. Murphy, T. H., Yu, J., Ng, R., Johnson, D. A., Shen, H., Honey, C. R., and Johnson, J. A. (2001) *J. Neurochem.* **76,** 1670–1678
42. Hardy, S., Kitamura, M., Harris-Stansil, T., Dai, Y., and Phipps, M. L. (1997) *J. Virol.* **71,** 1842–1849
43. Zipper, L. M., and Mulcahy, R. T. (2002) *J. Biol. Chem.* **277,** 36544–36552
44. Henthorn, P., Zervos, P., Raducha, M., Harris, H., and Kadesch, T. (1988) *Proc. Natl. Acad. Sci. U. S. A.* **85,** 6342–6346
45. Tietze, F. (1969) *Anal. Biochem.* **27,** 502–522
46. Guyot, M. C., Hantraye, P., Dolan, R., Palfi, S., Maziere, M., and Brouillet, E. (1997) *Neuroscience* **79,** 45–56
47. Brouillet, E., Guyot, M. C., Mittoux, V., Altairac, S., Conde, F., Palfi, S., and Hantraye, P. (1998) *J. Neurochem.* **70,** 794–805
48. Talalay, P., and Fahey, J. W. (2001) *J. Nutr.* **131,** 3027S–3033S
49. Talalay, P., Fahey, J. W., Holtzclaw, W. D., Prestera, T., and Zhang, Y. (1995) *Toxicol. Lett.* **82–83,** 173–179
50. Talalay, P., and Zhang, Y. (1996) *Biochem. Soc. Trans.* **24,** 806–810
51. Wu, L., Ashraf, M. H., Facci, M., Wang, R., Paterson, P. G., Ferrie, A., and Juurlink, B. H. (2004) *Proc. Natl. Acad. Sci. U. S. A.* **101,** 7094–7099
52. Nguyen, T., Huang, H. C., and Pickett, C. B. (2000) *J. Biol. Chem.* **275,** 15466–15473
53. Hayes, J. D., Chanas, S. A., Henderson, C. J., McMahon, M., Sun, C., Moffat, G. J., Wolf, C. R., and Yamamoto, M. (2000) *Biochem. Soc. Trans.* **28,** 33–41
54. Chanas, S. A., Jiang, Q., McMahon, M., McWalter, G. K., McLellan, L. I., Elcombe, C. R., Henderson, C. J., Wolf, C. R., Moffat, G. J., Itoh, K., Yamamoto, M., and Hayes, J. D. (2002) *Biochem. J.* **365,** 405–416
55. Chan, J. Y., and Kwong, M. (2000) *Biochim. Biophys. Acta* **1517,** 19–26
56. Kwak, M. K., Itoh, K., Yamamoto, M., Sutter, T. R., and Kensler, T. W. (2001) *Mol. Med.* **7,** 135–145
57. McWalter, G. K., Higgins, L. G., McLellan, L. I., Henderson, C. J., Song, L., Thornalley, P. J., Itoh, K., Yamamoto, M., and Hayes, J. D. (2004) *J. Nutr.* **134,** 3499S–3506S
58. Bjelke, B., England, R., Nicholson, C., Rice, M. E., Lindberg, J., Zoli, M., Agnati, L. F., and Fuxe, K. (1995) *Neuroreport* **6,** 1005–1009
59. Zoli, M., Jansson, A., Sykova, E., Agnati, L. F., and Fuxe, K. (1999) *Trends Pharmacol. Sci.* **20,** 142–150
60. Eftekharpour, E., Holmgren, A., and Juurlink, B. H. (2000) *Glia* **31,** 241–248
61. Olsen, C., Rustad, A., Fonnum, F., Paulsen, R. E., and Hassel, B. (1999) *Brain Res.* **850,** 144–149
62. McMahon, M., Itoh, K., Yamamoto, M., and Hayes, J. D. (2003) *J. Biol. Chem.* **278,** 21592–21600
63. Cullinan, S. B., Zhang, D., Hannink, M., Arvisais, E., Kaufman, R. J., and Diehl, J. A. (2003) *Mol. Cell. Biol.* **23,** 7198–7209
64. Calkins, M. J., Jakel, R. J., Johnson, D. A., Chan, K., Kan, Y. W., and Johnson, J. A. (2005) *Proc. Natl. Acad. Sci. U. S. A.* **102,** 244–249
65. Nguyen, T., Sherratt, P. J., and Pickett, C. B. (2003) *Annu. Rev. Pharmacol. Toxicol.* **43,** 233–260
66. Owuor, E. D., and Kong, A. N. (2002) *Biochem. Pharmacol.* **64,** 765–770
67. McMahon, M., Itoh, K., Yamamoto, M., Chanas, S. A., Henderson, C. J., McLellan, L. I., Wolf, C. R., Cavin, C., and Hayes, J. D. (2001) *Cancer Res.* **61,** 3299–3307
68. Ahlgren-Beckendorf, J. A., Reising, A. M., Schander, M. A., Herdler, J. W., and Johnson, J. A. (1999) *Glia* **25,** 131–142
69. Johnson, D. A., Andrews, G. K., Xu, W., and Johnson, J. A. (2002) *J. Neurochem.* **81,** 1233–1241
70. Rahimtula, A. D., Jernstrom, B., Dock, L., and Moldeus, P. (1982) *Br. J. Cancer* **45,** 935–944
71. Calne, D. B., Eisen, A., McGeer, E., and Spencer, P. (1986) *Lancet* **2,** 1067–1070
72. Di Monte, D. A., Lavasani, M., and Manning-Bog, A. B. (2002) *Neurotoxicology* **23**, 487–502
73. Jenner, P. (2001) *Trends Neurosci.* **24,** 245–247
74. FAO/WHO (1975) *FAO Nutr. Meet. Rep. Ser.* **55A,** 1–204
75. FAO/WHO (1997) *Natl. Toxicol. Program Tech. Rep. Ser.* **459,** 1–326
76. Cho, H. Y., Jedlicka, A. E., Reddy, S. P., Zhang, L. Y., Kensler, T. W., and Kleeberger, S. R. (2002) *Am. J. Respir. Cell Mol. Biol.* **26,** 42–51
77. Kensler, T. W., Davidson, N. E., Groopman, J. D., Roebuck, B. D., Prochaska, H. J., and Talalay, P. (1993) *Basic Life Sci.* **61,** 127–136
78. Fahey, J. W., Zhang, Y., and Talalay, P. (1997) *Proc. Natl. Acad. Sci. U. S. A.* **94,** 10367–10372
79. Fahey, J. W., Zalcmann, A. T., and Talalay, P. (2001) *Phytochemistry* 56, 5–51
80. Wu, L., and Juurlink, B. H. (2001) *J. Hypertens.* **19,** 1819–1825
81. Walz, W. (2000) *Glia* **31,** 95–103
82. Drukarch, B., Schepens, E., Stoof, J. C., Langeveld, C. H., and Van Muiswinkel, F. L. (1998) *Free Radic. Biol. Med.* **25,** 217–220
83. Zhou, F. M., Wilson, C. J., and Dani, J. A. (2002) *J. Neurobiol.* **53,** 590–605

Supplementary Figure 1. Behvioural scores and weight are highly correlated with lesion volume during 3-NP challenge. A B.)
Lesion volume was plotted against either behavioural scores obtained 1.5 days after the last 3-NP injection or percentage start weight 1.5 days after the last 3-NP injection. Strong correlations were found with both comparisons. Data represent the mean + SEM (animals per genotype: Nrf2+/+ = 5, Nrf2+/- = 7, Nrf2-/- =5). *** $p < 0.0001$, $r = 0.867$ (A), ** $p < 0.001$, $r = -0.693$ (B), Spearman test.

Supplementary Figure 2. RT-PCR images were collected within the linear range of the PCR reaction.
RNA extracted from vehicle, 3-NP treated glia (3 and 30 mM) was used for standard semi-quantitative RT-PCR.Appropriate primers were used to determine relative quantities of Nrf2, NQO1, GCLC, xCT transcripts, and these values were normalized with actin density **(A-D). E.)** 3-NP treatment did not affect actin mRNA levels. cDNA templates were serially diluted to ensure that band intensities were observed within the linear range of the PCR reaction. Densitometric analyses were performed with ImageJ Software (NIH). Data shown is representative of 3 independent experiments with similar results.

Supplementary Figure 1

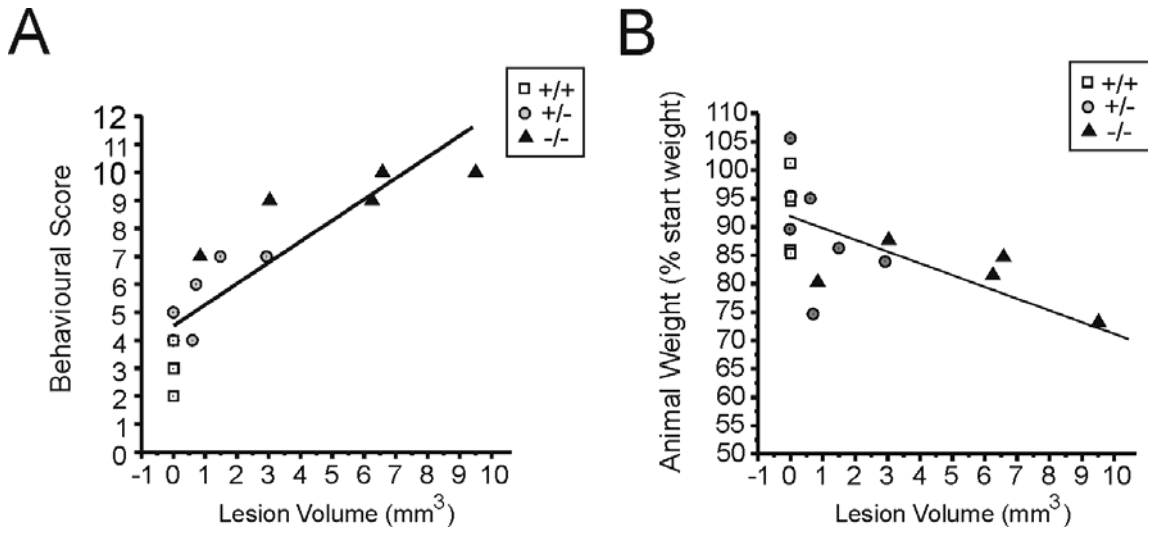

Supplementary Figure 2